

Phenomenological approach to transport through three-terminal disordered wires

A. M. Martínez-Argüello,^{1,*} J. A. Méndez-Bermúdez,^{1,†} and M. Martínez-Mares^{2,‡}

¹*Instituto de Física, Benemérita Universidad Autónoma de Puebla,
Apartado Postal J-48, 72570 Puebla, Mexico*

²*Departamento de Física, Universidad Autónoma Metropolitana-Iztapalapa,
Apartado Postal 55-534, 09340 Ciudad de México, Mexico*

We study the voltage drop along three-terminal disordered wires in all transport regimes, from the ballistic to the localized regime. This is performed by measuring the voltage drop on one side of a one-dimensional disordered wire in a three-terminal set-up as a function of disorder. Two models of disorder in the wire are considered: (i) the one-dimensional Anderson model with diagonal disorder and (ii) finite-width bulk-disordered waveguides. Based on the known β -dependence of the voltage drop distribution of the three-terminal chaotic case, being β the Dyson symmetry index ($\beta = 1, 2$, and 4 for orthogonal, unitary, and symplectic symmetries, respectively), the analysis is extended to a continuous parameter $\beta > 0$ and use the corresponding expression as a phenomenological one to reach the disordered phase. We show that our proposal encompasses all the transport regimes with β depending linearly on the disorder strength.

PACS numbers: 73.23.-b, 73.21.Hb, 72.10.-d, 72.15.Rn

I. INTRODUCTION

Quantum transport through multiprobe mesoscopic systems and nanostructures with complex dynamics has been of great interest for a long time (see for instance Refs. [1–11] and references therein). The earlier experiments considered conductors of normal metal whose size is larger than the elastic mean free path. Quantum coherence along the sample with randomly distributed impurities gives rise to striking quantum interference effects, as well as to sample-to-sample fluctuations in the transport properties, due to the different microscopic configurations of disorder, that were the subject of intense research like the magnetoresistance, the Hall effect, persistent currents, among others.^{12–15} More recently, the statistical fluctuations of the transport properties through clean quantum devices with chaotic classical dynamics, have been investigated.^{16–19}

Of particular interest are three-terminal systems since they offer potential applications;^{20,21} for instance, three terminal systems are used to sense the coupling strength between individual leads and the different modes in the device they are coupled to.²² The fluctuations of the voltage drop along an electronic device was first studied in disordered wires,^{3,4} while in chaotic devices was considered in Ref. [23], using random matrix theory simulations. For the particular configuration of the three-terminals, where the voltage probe is on one side of the chaotic wire, an analytical expression for all symmetry classes (orthogonal, unitary and symplectic) as well as an auxiliary experiment with chaotic microwave graphs that verifies the theoretical prediction, were presented in Ref. [24].

In this paper we study the voltage drop on one side of disordered wires for all the transport regimes. The system is studied by the scattering matrix approach and, in order to validate our results, we appeal to two models to describe the disordered wire: The finite size one-

dimensional Anderson model with diagonal disorder and finite-width bulk-disordered waveguides. Our analysis is based on the distribution of the voltage drop, whose dependence on the Dyson parameter β is explicit ($\beta = 1$ for the orthogonal symmetry, $\beta = 2$ for the unitary one, and $\beta = 4$ for the symplectic symmetry). This distribution is extended to continuous β , which is used as a phenomenological expression. We show that this procedure describes all transport regimes, deep from the ballistic to the localized regime, where the Dyson parameter β may be interpreted as the degree of disorder since it depends only on the ratio between the localization length and the system size, which is a measure of disorder. Our results are in agreement with numerical simulations and may be verified experimentally in single-mode waveguides with either bulk or surface disorder.

The paper is organized as follows. In Sect. II we summarize the main results about the voltage drop in three-terminal devices when the voltage probe is on one side of a horizontal disordered wire. Also, there, we present the corresponding statistical distribution and emphasize the Dyson parameter dependence when the wire is a chaotic cavity. In Sect. III we present the description of the disordered wire in terms of the open one-dimensional Anderson model, while a finite-width bulk-disordered waveguide realization is presented in Sect. IV. We present our conclusions in Sect. V.

II. VOLTAGE DROP IN A THREE-TERMINAL DEVICE

In the Landauer-Büttiker formalism of multi-terminal devices the electronic transport is reduced to a scattering problem.¹ The simplest arrangement that allows the measurement of the voltage drop along a device is a three-probe setting. As an example we consider the system shown in Fig. 1 in which the device, represented by the

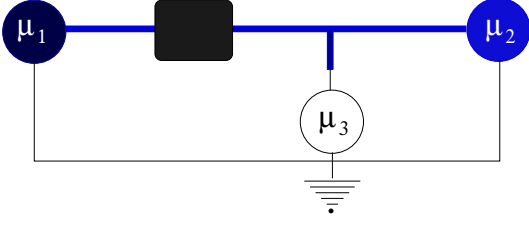


FIG. 1. Sketch of a three-probe setting that allows the measurement of the voltage drop along a device, represented by the horizontal wire. A flux current is established along the horizontal wire, while the vertical wire measures the voltage drop μ_3 , which depends on the chemical potentials μ_1 and μ_2 . The thin blue lines represent perfect conductors connected to the sources of voltages.

black box, is connected via perfect leads (blue lines) to fixed sources of voltages $\mu_1 (= eV_1)$ and $\mu_2 (= eV_2)$ that induce a flux current along the wire. The voltage drop can be measured by means of a third wire (vertical blue line) used as a voltage probe. This can be achieved by fulfilling the requirement that the current passing through the probe vanishes, thus yielding to the voltage drop $\mu_3 (= eV_3)$ along the device, namely²

$$\mu_3 = \frac{1}{2}(\mu_1 + \mu_2) + \frac{1}{2}(\mu_1 - \mu_2)f, \quad (1)$$

with

$$f = \frac{T_{31} - T_{32}}{T_{31} + T_{32}}, \quad (2)$$

where T_{31} and T_{32} are the partial transmission probabilities from wire 1 to wire 3 and from wire 2 to wire 3, respectively.

Since the electrons travel freely through each perfect lead and suffer a scattering process due to the disordered wire, the quantity f depends on the intrinsic nature of the conductor and contains all the relevant information about the multiple scattering in the device. If the device is a disordered or a chaotic wire, f fluctuates in the interval $[-1, 1]$ since μ_3 can not reach neither the value μ_1 nor μ_2 due to the contact resistance.²

We are interested in the situation in which the perfect leads are single-mode waveguides and that the probe is symmetrically coupled to the other two terminals at the junction. In that case the scattering matrix that describes the wire is a 2×2 matrix which has the general form

$$S = \begin{pmatrix} r & t' \\ t & r' \end{pmatrix}, \quad (3)$$

where r (r') and t (t') are the reflexion and transmission amplitudes when incidence is from the left (right) of the wire, and Eq. (2) takes the form²⁴

$$f = \frac{|t|^2 - |1 - r'|^2}{|t|^2 + |1 - r'|^2}. \quad (4)$$

A. Chaotic wire

For the case in which the wire is a chaotic cavity, S is chosen from an appropriate ensemble of scattering matrices according to the symmetry present in the system. That is, S belongs to one of the so-called circular ensembles from random matrix theory, with β representing the symmetry class present in the system: In the absence of any symmetry, flux conservation condition is the only requirement S must fulfill, it becomes a unitary matrix, $SS^\dagger = \mathbb{1}$ with $\mathbb{1}$ the 2×2 unit matrix, and S belongs to the Circular Unitary Ensemble (CUE). The presence of time reversal symmetry defines the Circular Orthogonal Ensemble (COE), in which case S is a symmetric unitary matrix, $S = S^T$, where T stands for the transpose. Finally, the presence of time reversal and spin-rotation symmetries define the Circular Symplectic Ensemble (CSE), in which S is a self-dual quaternion matrix and satisfies $S^R = S$ and the flux conservation condition reads $SS^* = \mathbb{1}$, where S^* is the complex quaternion of S . In the Dyson scheme, these ensembles are labeled by $\beta = 1, 2$, and 4 , respectively.²⁵ For these symmetry classes, the statistical distribution of f is given by²⁴

$$p_\beta(f) = \begin{cases} \frac{1}{\pi} \sqrt{(1-f)/(1+f)} & \text{for } \beta = 1, \\ \frac{1}{2}(1-f) & \text{for } \beta = 2, \\ \frac{3}{4}(1+f)(1-f)^2 & \text{for } \beta = 4, \end{cases} \quad (5)$$

which can be written in a single equation as

$$p_\beta(f) = 2^{1-\beta} \frac{\Gamma(\beta)}{[\Gamma(\beta/2)]^2} \frac{(1-f)^{\beta/2}}{(1+f)^{1-\beta/2}}. \quad (6)$$

This distribution is the main quantity on which this paper is focused. We propose $p_\beta(f)$ of Eq. (6) as a phenomenological expression where the index β is extended to a continuous parameter that allows to cover all transport regimes, from the ballistic to deep in the localized regime. To verify the validity of our assertion we make use of two models for the description of the disorder in the wire: The open one-dimensional Anderson model and finite-width bulk-disordered waveguides.

III. OPEN 1D ANDERSON MODEL: EFFECTIVE HAMILTONIAN APPROACH

A model of disorder in the wire can be implemented in an N -site one-dimensional wire of length L described by the tight-binding Hamiltonian H with nearest neighbor interactions of the form

$$H_{mn} = \varepsilon_n \delta_{mn} - \nu(\delta_{m,n+1} + \delta_{m,n-1}), \quad (7)$$

where ε_n is the energy of site n , ν is the tunnel transition amplitude to nearest neighbor sites, and δ is the usual Kronecker delta. For diagonal disorder ν is just

a constant, that we fix to $\nu = 1$, while the site energy ε_n is a random number which for simplicity we consider uniformly distributed in the interval $[-w/2, w/2]$ with variance $\sigma^2 = \langle \varepsilon_n^2 \rangle = w^2/12$, being w a measure of the amount of disorder.

We open the wire by attaching it on the left ($L = 1$) and right ($L = N$) ends to semi-infinite single-mode perfect leads with coupling strength $\gamma^{L,R}$ to the left (L) and to the right (R) end, respectively. The 2×2 S -matrix can be written in the form⁷

$$S(E) = \mathbb{1} - 2i \sin(k) W^T \frac{1}{E - \mathcal{H}_{\text{eff}}} W \quad (8)$$

where E is the energy, $k = \arccos(E/2)$ is the wave vector supported in the leads, and \mathcal{H}_{eff} is the effective non-Hermitian Hamiltonian, namely

$$\mathcal{H}_{\text{eff}} = H - \frac{e^{ik}}{2} W W^T. \quad (9)$$

In Equations (8) and (9) the matrix $W(E)$ describes the coupling of the wire with the leads. Its elements are defined by

$$W_{mn} = 2\pi \sum_{c=L,R} A_m^c(E) A_n^c(E), \quad (10)$$

with the coupling amplitudes

$$A_n^{L,R}(E) = \sqrt{\frac{\gamma^{L,R}}{\pi}} \left(1 - \frac{E^2}{4}\right)^{1/4} (\delta_{n,1}^L + \delta_{n,N}^R). \quad (11)$$

Furthermore, the energy dependence in \mathcal{H}_{eff} can be neglected since $\arccos(E/2)$ changes slightly at the center of the band. Moreover, the inverse localization length reduces to $\ell_{\infty}^{-1}(E) = w^2/105.2$,²⁶ which means that the higher the intensity of disorder the smaller the localization length is, as expected.

From Eq. (8) we observe that the reflection and transmission amplitudes t and r' , respectively, that appear in the expression of f , Eq. (4), depend on the localization length and the degree of disorder. This dependence is only through the ratio $\xi = \ell_{\infty}/L$, from which ξ^{-1} (the length of wire in units of the localization length) can be considered as the disorder strength, satisfying a single-parameter scaling hypothesis.²⁷ This is verified in Fig. 2 for the distribution of T_{31} and T_{32} for different wire lengths.

In Fig. 3 we show the behavior of distribution $p_{\beta}(f)$ for several values of β for (a) the analytical expression, Eq. (6), and (b) numerical simulations of f with r' and t obtained from Eq. (8). The cases $\beta \approx 1, 2$, and 4 , indicated in the inset of panel (a), correspond roughly to the chaotic cases in presence and absence of time-reversal invariance, and in presence of symplectic symmetry; respectively. The fitting between the analytical expression $p_{\beta}(f)$ to the numerical distribution, for each value of the ratio ξ , determines the corresponding value of β . We numerically found that the parameters ξ and β are related

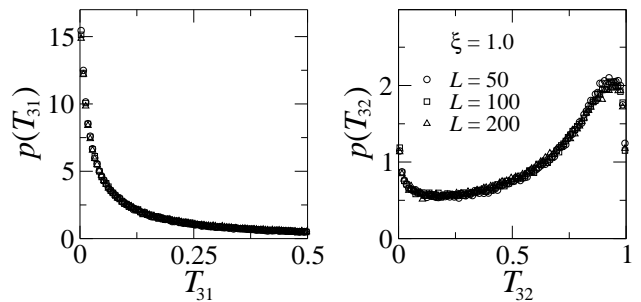


FIG. 2. Distribution of T_{31} and T_{32} for a fixed ξ and different wire lengths, as indicated in the panels. For the numerical calculation we used an ensemble of 2×10^5 wire realizations and 100 bins to construct the histograms.

through a quadratic equation given by

$$\beta(\xi) \approx -4.449 \times 10^{-3} \xi^2 + 1.071 \xi - 0.1806, \quad (12)$$

with a statistical indicator of $\chi^2 = 4.34 \times 10^{-4}$, as shown in the inset of Fig. 3 (b). For the fitting we chose ξ in the interval $[1.7, 3.7]$ in order to avoid divergencies for values of f close to -1. Furthermore, in Fig. 3 we observe some deviations between both distributions which are model-dependent, however the phenomenology showed by the expression of Eq. (6) is well reproduced. A continuous transition between different values of β is also observed. For the simulations we constructed ensembles of 2×10^5 disordered wires and used 100 bins to construct the histograms.

In what follows we verify our proposal with a more realistic model of disorder, i.e., with finite-width bulk-disordered waveguides.

IV. APPLICATION TO BULK-DISORDERED WAVEGUIDES

We validate the applicability of our proposal, Eq. (6), by means of finite element simulations of bulk-disordered (BD) waveguides. A BD waveguide consists of a quasi-one-dimensional wire formed by attaching N two-dimensional building blocks (BB). Every building block is a square cavity of side d connected to two semi-infinite leads of width d on the left and right sides. We place at

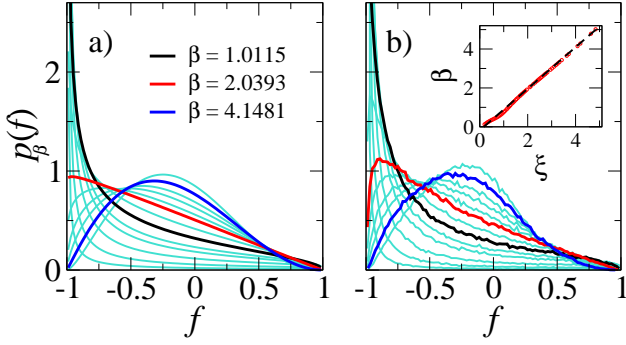


FIG. 3. (Color online) Behavior of $p_\beta(f)$ for several values of β for (a) the analytical expression, Eq. (6), and (b) for numerical simulations of Eq. (8) with disorder modeled by the 1D Anderson Hamiltonian. The $\beta \approx 1, 2$ and 4 cases, indicated in the inset of panel (a), correspond to the chaotic cases in presence and absence of time-reversal invariance, and presence of symplectic symmetry; respectively. In the inset of panel (b) we show the relationship between ξ and β obtained by fitting $p_\beta(f)$ to the numerical distributions (see the text).

random a circular obstacle of radius ρ inside each building block to produce an ensemble. The leads support plane waves with energy E ; when E lies inside the interval $(\hbar^2/2md^2) [\mu^2\pi^2, (\mu+1)^2\pi^2]$ they support μ open channels. We use the dimensionless units $\hbar^2/2md^2 = 1$, so that one open channel (i.e., the case we will focus below) occurs for $E \in [\pi^2, (2\pi)^2]$. We fix the energy to $E = (1.5\pi)^2$, so that both leads support one open channel and the energy is far from the new channel threshold in order to avoid threshold singularities; we also set $d = 100\rho_0$ with $\rho_0 = 1$.

To compute the scattering quantities of the bulk-disordered waveguides we use the combination rule of scattering and transfer matrices, as shown in Ref. [28]. First, by means of standard finite element methods (see for instance Refs. [29–31]) we compute the scattering matrix of a i -th building block:

$$S_{\text{BB}}^{(i)} = \begin{pmatrix} r_i & t'_i \\ t_i & r'_i \end{pmatrix}, \quad (13)$$

where r_i (r'_i) and t_i (t'_i) are the reflection and transmission amplitudes, for incidence from the left (right). Then, the transfer matrix is easily obtained from the elementary relation with the S -matrix,³² this relation leads to

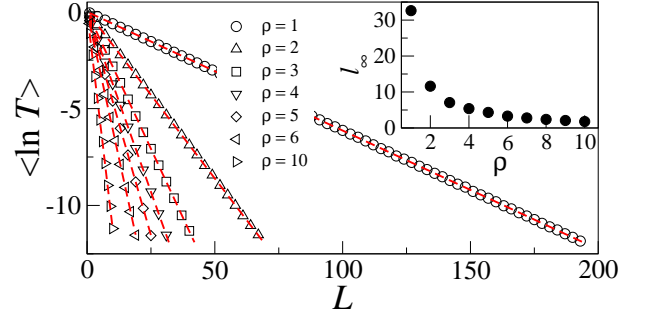


FIG. 4. (Color online) Average logarithm of the conductance $\langle \ln g \rangle$ as a function of the waveguide length L for bulk-disordered waveguides (supporting one open channel) characterized by $\rho = [1, 10]$. Red-dashed lines are fittings to the data with Eq. (17); these fittings are performed to extract the localization lengths ℓ_∞ . Inset: ℓ_∞ as a function of ρ . Each point in the figure is computed by averaging over an ensemble of 10^5 waveguide realizations.

the transfer matrix of the building block $M_{\text{BB}}^{(i)}$. Therefore, since the building blocks are attached in series, the transfer matrix M of the complete waveguide composed by $L = N$ building blocks can be easily calculated as

$$M(L) = \prod_{i=1}^L M_{\text{BB}}^{(i)} = \begin{pmatrix} \alpha & \beta \\ \beta^* & \alpha^* \end{pmatrix}. \quad (14)$$

Finally, the scattering matrix of the waveguide of length L is

$$S(L) = \frac{1}{\alpha^*} \begin{pmatrix} -\beta^* & 1 \\ 1 & \beta \end{pmatrix} = \begin{pmatrix} r & t' \\ t & r' \end{pmatrix}. \quad (15)$$

For the statistical analysis we generate an ensemble of bulk-disordered waveguides from sets of different building blocks, constructed by randomly moving the inner obstacle of radius ρ . In Fig. 4 we plot the average of $\langle \ln T \rangle$, where T is given by^{1,2,33,34}

$$T(L) = \text{tr}(tt'), \quad (16)$$

as a function of the waveguide length L for bulk-disordered waveguides with $\rho = [1, 10]$. Notice that the decay of $\langle \ln T \rangle$ vs. L is faster the larger the value of ρ . Thus one can use the radius of the obstacle to tune the disorder strength in our waveguides: The larger the value

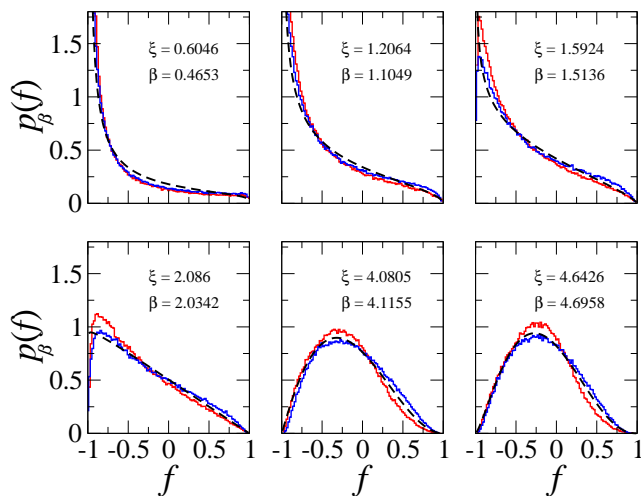


FIG. 5. (Color online) Probability distribution, $p_\beta(f)$, for the three-terminal disordered device. The histograms correspond to the distribution of f , Eq. (4), with r' and t obtained from numerical simulations for the 1D Anderson model (red) and for bulk-disordered waveguides (blue). For the numerical analysis we performed ensembles of 2×10^5 wire realizations. For the histograms we used 100 bins.

of ρ the stronger the disorder strength. Furthermore, by fitting these curves to³⁵

$$\langle \ln T \rangle = -2L/\ell_\infty = -2/\xi, \quad (17)$$

we extract the corresponding localization length ℓ_∞ , see red dashed lines in Fig. 4. In the inset of Fig. 4 we show the obtained values of ℓ_∞ as a function of ρ . They are used to design waveguides characterized by specific disorder strengths through the ratio $\xi = \ell_\infty/L$. We restrict our analysis to building blocks with inner obstacles with radius $\rho = 1$ to get longer waveguides (see Fig. 4), but since the lengths L of the waveguides are given as integer multiples of building blocks, not any value of ξ is allowed.

In Fig. 5 we present probability distributions $p_\beta(f)$ for the three-terminal disordered device for different values of ξ , as indicated in the insets. The dashed lines correspond to the analytical expression, Eq. (6), with β obtained from Eq. (12) for the corresponding ξ . The

histograms correspond to the numerical results obtained from the two models of the disordered wire, the 1D Anderson model of Eq. (8) (red) and for bulk-disordered waveguides of Eq. (15) (blue). The results show significant model-dependent deviations, however the phenomenology captured by $p_\beta(f)$ is well reproduced for all the transport regimes.

V. CONCLUSIONS

We studied the voltage drop along a horizontal disordered wire, in a three-terminal device. The voltage was measured by means of a third terminal, used as a voltage probe, in an asymmetric configuration; that is, when the probe is on one side of the wire. Our analysis was based on a random matrix theory result accounting for the distribution of the voltage $p_\beta(f)$, depending only on the Dyson parameter β for all symmetry classes: orthogonal ($\beta = 1$), unitary ($\beta = 2$), and symplectic ($\beta = 4$). This distribution was extended to a continuous parameter $\beta > 0$ and proposed as a phenomenological expression covering all the transport regimes of the disordered wire, from the ballistic to the localized regime. We validate our proposal with two models for the disordered wire: The one-dimensional Anderson model and bulk-disordered waveguides. It is relevant to stress that the parameter β in $p_\beta(f)$ may be interpreted as the (reciprocal) degree of disorder in a wire of length L , and characterized by the localization length ℓ_∞ , since we found that $\beta \approx \ell_\infty/L$ in a wide range of disorder strengths. We have to admit that our results show significant deviations between the numerical distributions and our proposal, however the phenomenology is well reproduced.

It is worth mentioning that given the wide classical wave analogies to quantum transport,^{36–44} our results can be tested by experiments with microwaves or mechanical waves with either surface or bulk disordered waveguides.

ACKNOWLEDGMENTS

A.M.M.-A. acknowledges Benemérita Universidad Autónoma de Puebla (BUAP) and PRODEP under the project DSA/103.5/16/11850 for financial support. JAM-B acknowledges financial support from VIEP-BUAP (Grant No. MEBJ-EXC18-G), Fondo Institucional PIFCA (Grant No. BUAP-CA-169), and CONACyT (Grant No. CB-2013/220624). MM-M thanks to CONACyT financial support through the Grant No. CB-2016/285776.

* blitzkriegheinkel@gmail.com

† jmendez@ifuap.buap.mx

‡ moi@xanum.uam.mx

¹ M. Büttiker, Phys. Rev. Lett. **57**, 1761 (1986).

² M. Büttiker, IBM J. Res. Dev. **32**, 317 (1988).

³ S. Godoy and P. A. Mello, Europhys. Lett. **17**, 243 (1992).

⁴ S. Godoy and P. A. Mello, Phys. Rev. B **46**, 2346 (1992).

- ⁵ V. A. Gopar, M. Martínez, and P. A. Mello, Phys. Rev. B **50**, 2502 (1994).
- ⁶ A. M. Song, A. Lorke, A. Kriele, J. P. Kotthaus, W. Wegscheider, and M. Bichler, Phys. Rev. Lett. **80**, 3831 (1998).
- ⁷ S. Datta, *Electronic Transport in Mesoscopic Systems* (Cambridge University Press, Cambridge, 1995).
- ⁸ S. Goodnick, IEEE Transactions on Nanotechnology **2**, 368 (2003).
- ⁹ B. Gao, Y. F. Chen, M. S. Fuhrer, D. C. Glatli, and A. Bachtold, Phys. Rev. Lett. **95**, 196802 (2005).
- ¹⁰ L. Arrachea, Phys. Rev. B **77**, 233105 (2008).
- ¹¹ F. Foieri, L. Arrachea, and M. J. Sánchez, Phys. Rev. B **79**, 085430 (2009).
- ¹² R. A. Webb, S. Washburn, C. P. Umbach, R. B. Laibowitz, Phys. Rev. Lett. **54**, 2696 (1985).
- ¹³ M. A. Paalanena, D. C. Tsui, A. C. Gossard, J. C. M. Hwang, Solid State Comm. **50**, 841 (1984).
- ¹⁴ K. Saeed, N. A. Dodoo-Amoo, L. H. Li, S. P. Khanna, E. H. Linfield, A. G. Davies, and J. E. Cunningham, Phys. Rev. B **84**, 155324 (2011).
- ¹⁵ L. P. Lévy, G. Dolan, J. Dunsmuir, and H. Bouchiat, Phys. Rev. Lett. **64**, 2074 (1990).
- ¹⁶ C. M. Marcus, A. J. Rimberg, R. M. Westervelt, P. F. Hopkins, and A. C. Gossard, Phys. Rev. Lett. **69**, 506 (1992).
- ¹⁷ C. W. J. Beenakker, Rev. Mod. Phys. **69**, 731 (1997).
- ¹⁸ Y. Alhassid, Rev. Mod. Phys. **72**, 895 (2000).
- ¹⁹ P. A. Mello and H. Baranger, *Interference phenomena in electronic transport through chaotic cavities: An information-theoretic approach* in *The XXXI latin american school of physics (Escuela Latinoamericana de Física, ELAF) new perspectives on quantum mechanics*, AIP Conf. Proc. **464**, 281 (1999).
- ²⁰ A. Jacobsen, I. Shorubalko, L. Maag, U. Sennhauser, and K. Ensslin, Appl. Phys. Lett. **97**, 032110 (2010).
- ²¹ A. N. Jordan and M. Büttiker, Phys. Rev. B **77**, 075334 (2008).
- ²² A. Jacobsen, P. Simonet, K. Ensslin, and T. Ihn, New J. Phys. **14**, 023052 (2012).
- ²³ A. M. Martínez-Argüello, E. Castaño, and M. Martínez-Mares, *Random matrix study for a three-terminal chaotic device* in *Special Topics on Transport Theory: Electrons, Waves, and Diffusion in Confined Systems*, AIP Conf. Proc. **1579**, 46 (2014).
- ²⁴ A. M. Martínez-Argüello, A. Rehemangiang, M. Martínez-Mares, J. A. Méndez-Bermúdez, H.-J. Stöckmann, and U. Kuhl, Phys. Rev. B **98**, 075311 (2018).
- ²⁵ F. J. Dyson, *J. Math. Phys.* **3**, 140 (1962).
- ²⁶ M. Kappus and F. Wegner, Z. Phys. B: Condens. Matter. **45**, 15 (1981).
- ²⁷ P. W. Anderson, D. J. Thouless, E. Abrahams, and D. S. Fisher, Phys. Rev. B **22**, 3519 (1980).
- ²⁸ A. Alcázar-López, J. A. Méndez-Bermúdez, and G. A. Luna-Acosta, J. Phys.: Conf. Series **475**, 012001 (2013).
- ²⁹ G. A. Luna-Acosta, J. A. Méndez-Bermúdez, P. Šeba, and K. N. Pichugin, Phys. Rev. E **65**, 046605 (2002).
- ³⁰ J. A. Méndez-Bermúdez, G. A. Luna-Acosta, P. Šeba, and K. N. Pichugin, Phys. Rev. E **66**, 046207 (2002).
- ³¹ J. A. Méndez-Bermúdez, G. A. Luna-Acosta, P. Šeba, and K. N. Pichugin, Phys. Rev. B **67**, 161104 (2003).
- ³² P. A. Mello and N. Kumar, *Quantum Transport in Mesoscopic Systems: Complexity and Statistical Fluctuations* (Oxford University Press, New York, 2005).
- ³³ R. Landauer, IBM J. Res. Dev. **1**, 223 (1957).
- ³⁴ R. Landauer, IBM J. Res. Dev. **32**, 336 (1988).
- ³⁵ P. W. Anderson, Phys. Rev. **109**, 1492 (1958).
- ³⁶ E. Doron, U. Smilansky, and A. Frenkel, Phys. Rev. Lett. **65**, 3072 (1990).
- ³⁷ R. A. Méndez-Sánchez, U. Kuhl, M. Barth, C. H. Lewenkopf, H.-J. Stöckmann, Phys. Rev. Lett. **91**, 174102 (2003).
- ³⁸ H. Schanze, H.-J. Stöckmann, M. Martínez-Mares, C. H. Lewenkopf, Phys. Rev. E **71**, 016223 (2005).
- ³⁹ U. Kuhl, M. Martínez-Mares, R. A. Méndez-Sánchez, H.-J. Stöckmann, Phys. Rev. Lett. **94**, 144101 (2005).
- ⁴⁰ S. Hemmady, X. Zheng, E. Ott, T. M. Antonsen, Jr., S. M. Anlage, Phys. Rev. Lett. **94**, 014102 (2005).
- ⁴¹ D. Laurent, O. Legrand, F. Mortessagne, Phys. Rev. E **74**, 046219 (2006).
- ⁴² S. Bittner, B. Dietz, M. Miski-Oglu, P. O. Iriarte, A. Richter, F. Schäfer, Phys. Rev. E **84**, 016221 (2011).
- ⁴³ A. M. Martínez-Argüello, M. Martínez-Mares, M. Cobián-Suárez, G. Báez, and R. A. Méndez-Sánchez, EPL **110**, 54003 (2015).
- ⁴⁴ E. Flores-Olmedo, A. M. Martínez-Argüello, M. Martínez-Mares, G. Báez, J. A. Franco-Villafañe, and R. A. Méndez-Sánchez, Sci. Rep. **6**, 25157 (2016).